

# UC Irvine

## UC Irvine Previously Published Works

### Title

Ultra-deep imaging of turbid samples by enhanced photon harvesting

### Permalink

<https://escholarship.org/uc/item/9442v106>

### ISBN

9780819493576

### Authors

Crosgnani, Viera  
Dvornikov, Alexander  
Gratton, Enrico

### Publication Date

2013-02-22

### DOI

10.1117/12.2002101

### Copyright Information

This work is made available under the terms of a Creative Commons Attribution License, available at <https://creativecommons.org/licenses/by/4.0/>

Peer reviewed

# Ultra-deep imaging of turbid samples by enhanced photon harvesting

Viera Crosignani, Alexander Dvornikov, Enrico Gratton\*

Laboratory for Fluorescence Dynamics, Department of Biomedical Engineering, University of California Irvine, Irvine, California, USA

## ABSTRACT

We constructed an advanced detection system for two-photon fluorescence microscopy that allows us to image in biological tissue and tissue phantoms up to the depth of a few mm with micron resolution. The innovation lies in the detection system which is much more sensitive to low level fluorescence signals than the fluorescence detection configuration used in conventional two-photon fluorescence microscopes. A wide area photocathode photomultiplier tube (PMT) was used to detect fluorescence photons directly from a wide (1 inch diameter) area of the turbid sample, as opposed to the photon collection by the microscope objective which can only collect light from a relatively small area of the sample. The optical path between the sample and the photocathode is refractive index matched to curtail losses at the boundaries due to reflections. The system has been successfully employed in the imaging of tissue phantoms simulating brain optical properties and in biological tissues, such as murine small intestine, colon, tumors, and other samples. The system has in-depth fluorescence lifetime imaging (FLIM) capabilities and is also highly suitable for SHG signal detection, such as collagen fibers and muscles, due to the intrinsically forward-directed propagation of SHG photons.

**Keywords:** deep imaging, fluorescence, two-photon microscopy, FLIM, SHG

## 1. INTRODUCTION

The ability to visualize features in deep layers of biological tissue with high resolution is a very sought-after feature of an imaging system employed in medical diagnostics and in clinical and biological applications. Deep-tissue imaging has many applications, all based on the necessity of exploring cells and molecules in the intact organism, a sort of “optical pathology” that removes the need of biopsies and fixing, and grants access to structures and functions in the native physiological environment.

Both the geometrical and optical properties of the sample and the characteristics of the microscope system affect the achievable imaging depth. While transparent specimens can be easily imaged with a traditional microscope, biological tissue is an intrinsically turbid medium, which produces a strong multiple scattering, absorption and exhibits inhomogeneity of the refractive index. These features make traditional light and fluorescence microscopy, even with the aid of staining and the addition of fluorescent markers to improve contrast, ineffective past the 100-200  $\mu\text{m}$  surface layer of the sample [1].

In order to access deeper layer of turbid samples, high power, short pulse emitting lasers in the near infrared (NIR) are required. This allows taking advantage of reduced absorption and scattering at longer wavelengths. The advent of multi-photon microscopy has improved the achievable imaging depth, but the current microscope technology is still limited by an imaging depth of about 1 mm [2,3,4,5].

We have constructed a two-photon fluorescence microscope capable of imaging in turbid media simulating brain optical properties up to the depth of a few mm. Such an increased penetration depth is the result of a novel photon harvesting system which is able to collect emission photons from a wide area of the sample in contrast to the conventional detection scheme that collects photons only from a relatively small area, while most photons are lost. Light losses are also reduced by means of refractive index matching throughout the optical path. The system has proven extremely effective in imaging of many biological and artificial samples, such as murine colon and small intestine, vasculature in the skin, subcutaneous xenograft tumors in mice and various tissue phantoms.

\*egratton@uci.edu; phone 1 949 824-2674; fax 1 949 824-1727; www.lfd.uci.edu

Due to its transmission geometry, our imaging system is also extremely suitable for second harmonic generation (SHG) signal detection. SHG is a coherent process that produces photons at exactly half the wavelength of the excitation light. Second harmonic generation (SHG) is a useful optical tool for biological and medical imaging and diagnostics [6]. The physical process does not involve absorption to generate contrast, like in the case of multi-photon fluorescence microscopy, but arises from the polarization of specific endogenous structures lacking center of symmetry, thus not requiring staining of the sample. SHG also works with near IR lasers frequencies, which allows imaging at an increased depth in biological tissue with high resolution. Unlike fluorescence, which produces an isotropic emission, SHG mainly propagates in the direction of the excitation beam [7]. Because of its intrinsic forward-directed nature, SHG detection is better accomplished in an imaging system working in transmission geometry.

Its unique properties make SHG a very powerful imaging technique, both *ex vivo* and *in vivo*, and it has been successfully used in the imaging of diseases of connective tissue [8]. Collagen, the most abundant component of the extra-cellular matrix (ECM), generates a very strong second harmonic signal. Many diseases, such as ovarian [9] and breast cancer [10] are characterized by a remodeling of the ECM. Also myosin, present in large amounts in biological samples, gives a strong SHG signal and the imaging of the arrangement of the fibrils can give insight into many muscle diseases [11].

We were able to obtain SHG images of biological and non-biological specimens in depth using very low excitation light power, and thus causing less photo-damage, when compared to traditional microscope geometry.

Our system is also equipped with a FLIMBox that allows in depth fluorescence lifetime imaging (FLIM). FLIM is a powerful imaging technique that maps the spatial distribution of the unique lifetimes of intrinsic and extrinsic fluorophores, such as NADH, FAD, and fluorescent proteins [12]. FLIM has many applications, such as the analysis of protein-protein interactions and to solve various biological problems [13,14]. Traditionally, FLIM analysis was performed in the time domain and has been very computationally demanding. The phasor-approach [15] introduced by Digman *et al.*, performs FLIM data analysis in the frequency domain and it has greatly simplified data processing.

## 2. EXPERIMENTAL

### 2.1 Imaging system

The imaging system is based on a custom made upright two photon excitation microscope with a unique emission detection method. The principles of operation were previously described [16,17]. Here we describe a modified system, shown schematically in Figure 1.

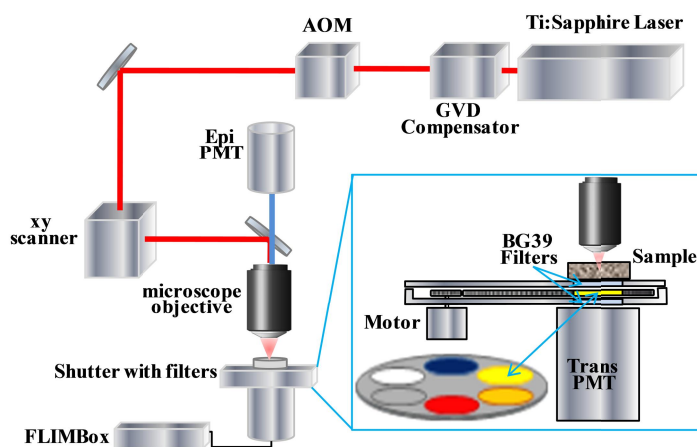


Figure 1. Schematic diagram of the experimental system

A tunable femtosecond pulsed Ti:Sa laser (Mai Tai, Spectra Physics) is used for two-photon fluorescence excitation and SHG. The laser is coupled to a group velocity dispersion compensator (DeepSee, Spectra Physics) to achieve maximum fluorescence excitation efficiency in the sample. An acousto-optic modulator (AOM, AA Opto-Electronics MT 110-B50A1) is used to adjust the power of the excitation beam. The beam is then directed to a x-y galvanometric scanner (ISS) coupled with an Olympus BX illumination module equipped with long working distance objectives (Olympus LCPlanFl 20x/0.4 and Olympus LUMPlanFl 40x/0.80 W). The sample is directly placed on the detection system in a transmission configuration (described below) attached to a motorized x-y-z stage used for positioning of the specimen and focusing.

The detector used in the transmission configuration is the key feature of the imaging system that allows us to image in turbid samples up to the depth of a few millimeters [16,17]. As it will be shown below, this system has also proven extremely efficient in the detection of SHG photons, due to their intrinsic forward directed propagation. The detector here described was modified by adding a filter wheel to separate the emission photons by wavelength. The detector comprises of a large photocathode area head-on PMT (Hamamatsu R7600P-300), working in photon counting mode, coupled to the shutter. The shutter is custom made of a sealed aluminum case that houses the filter wheel rotated by a stepper motor. The filter case is filled with index matching fluid to keep the optical path between the sample and the PMT window completely index matched. This minimizes losses of fluorescence and SHG photons caused by multiple reflections at the boundaries. This detection scheme allows the efficient collection of emission photons directly from the wide surface area of the sample, which makes it extremely sensitive to very low signal levels. The system is equipped with a FLIMBox (ISS) that allows fluorescence lifetime imaging microscopy (FLIM). The system is also equipped with a second PMT (Hamamatsu H7422P-40) that works in the epi-fluorescence configuration to compare the results between the conventional 2-photon fluorescence microscope configuration and our system.

## 2.2 Sample preparation

Silicone tissue phantoms (reduced scattering coefficient  $\mu_s' = 1.13 \text{ mm}^{-1}$  at 800nm excitation wavelength) were prepared according to [18] to which yellow-green (2  $\mu\text{m}$  and 15 $\mu\text{m}$ ) and red (10  $\mu\text{m}$ ) fluorescent beads (Invitrogen) were added. Samples were also prepared in the same way with the addition of urea crystals (Aldrich) for SHG experiments. Before being mixed with the polymer the urea crystals were powderized in a mortar. Two types of samples containing urea crystals were prepared: one type with a scattering agent ( $\text{TiO}_2$ ) and the other without scattering agent (clear). The sample dimensions are 35 mm in diameter by 8 mm thickness.

Samples of cells embedded in collagen matrix were prepared as following. Type I collagen was purchased from BD Biosciences (Franklin Lakes, NJ), with original concentration of 3.75mg/ml. Collagen was diluted with 10X PBS with phenol red and water to a final concentration of 1X PBS and 2mg/ml collagen solution. NaOH was added to neutralize the collagen solution before mixing it with cells. Fluorescent labeled paxillin MDA-MB-231 cells in serum free DMEM were mixed with 2mg/ml collagen solution, with the final concentration of  $5 \times 10^4$  cells/ml. The collagen/cell mixture was polymerized at 20°C for 1 hr and then at 37°C for 20 min. Full medium was applied after polymerization. Measurements were performed 2 to 4 days after the cells were cultured in the collagen matrix.

Samples of murine colon and small intestine were prepared according to [19]. The rodent dorsal chamber procedures can be found in [20]. Xenograft tumors grown subcutaneously in immune-deficient mice were excised from a skin flap and immediately imaged. The mouse was euthanized right after the removal of the tumor.

## 3. RESULTS AND DISCUSSION

### 3.1 Imaging of turbid samples

We have previously [16,17] demonstrated that by employing the described detection scheme images of fluorescent beads in turbid samples could be acquired up to the depth of 3 mm, while a commercial Zeiss LSM 710 microscope could image the same samples only to a depth of 500  $\mu\text{m}$ . Our system has been ameliorated by the addition of a more

powerful laser and a group velocity dispersion compensation device, allowing us to further increase the imaging depth. To demonstrate the in-depth imaging capabilities of the system we have imaged 2  $\mu\text{m}$  yellow-green fluorescent beads dispersed in a tissue phantom with brain-like optical properties.

Figure 2a shows the image of the bead acquired at 3.5 mm depth with a 20x 0.4 NA air objective. The same sample could only be imaged up to about 500  $\mu\text{m}$  depth in the epi-fluorescence configuration on a commercial Zeiss LSM 710 or with the epi-PMT on our system using the same objective and excitation parameters. In spite of the significant depth, high-resolution was preserved in the image. The image size presented in the figure corresponds to the actual size of the bead, confirming the high resolution in-depth imaging capability of the system. Figure 2b shows the image of a cluster of 2  $\mu\text{m}$  beads placed between two scattering slices of silicone resin 4 mm thick each. For this turbid sample the image quality at a 4 mm imaging depth decreases, and more frames need to be accumulated and averaged to keep a given image quality. However, the individual beads can be clearly resolved and seen in the acquired image.

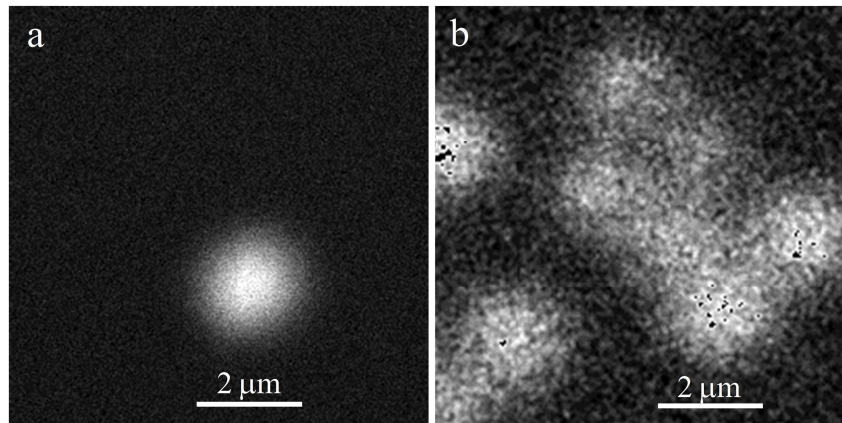


Figure 2. Image of a 2  $\mu\text{m}$  yellow-green fluorescent bead embedded in silicone tissue phantom acquired at 3.5mm depth (a); cluster of beads placed between 4mm thick slices of scattering media (b). Excitation wavelength 800 nm.

Biological tissue is intrinsically a very turbid medium, due to strong scattering and also to the inhomogeneity of the refractive index, which varies significantly between tissues [21]. This will strongly affect the maximum achievable imaging depth that will also vary according to tissue optical properties. However, our detection system, due to its high sensitivity and ability to collect more emission photons from the wide area of the sample, makes it possible to image deeper in such tissues than conventional two-photon microscopes that utilize the epi-fluorescence detection scheme.

We have imaged blood vessels contrasted with FITC-Dextran in various biological tissues, such as murine colon, subcutaneous xenograft tumor in immune-deficient mouse and *in vivo* in skin in rodent dorsal chamber (Figure 3). While the commercial Zeiss LSM 710 microscope could image the same samples to depths not exceeding 170  $\mu\text{m}$ , we were able to image 4-5 times deeper using our detection method.

Figure 3a shows the *ex vivo* image of 3D-reconstruction of blood vessels in murine colon, imaged to 350  $\mu\text{m}$  depth. Cell growth, proliferation, and differentiation are connected to the degree of oxygenation of the cells and their surrounding tissue. Since oxygen is delivered to tissues by the vasculature, it is of great interest to image the vasculature at the bottom of the crypts in order to establish a relationship between cell behavior/metabolism and proximity to the oxygen source [22].

Tumors grow a vasculature network to supply oxygen and nutrition. The ability to image the vasculature can provide important insight into the progression of the tumor. Figure 3b shows the *ex vivo* image of blood vessels in a subcutaneous xenograft tumor in an immune-deficient mouse, acquired at 630  $\mu\text{m}$  depth.

Figure 3c shows image of blood vessels in the skin acquired *in vivo* in a rodent dorsal chamber at 560  $\mu\text{m}$  depth. Unlike the usual use of this chamber [20], where the blood vessels are imaged from the side where the skin was excised

to expose the blood vessels, we were able to image the blood vessels from the intact skin side throughout the thickness of the specimen, a task that cannot be accomplished with a conventional microscope. Avoiding the skin excision step noticeably cuts down the surgery time, greatly decreases the risk of infections, and inflicts less suffering on the specimen.

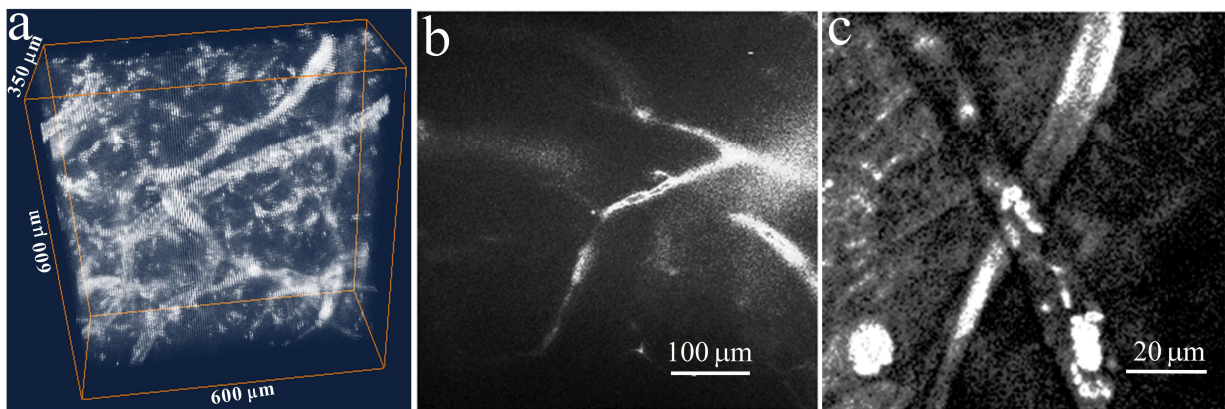


Figure 3. Images of blood vessels with FITC-Dextran as a contrast agent. a) murine colon b) subcutaneous xenograft tumor in immune-deficient mouse, depth 630 μm c) skin in rodent dorsal chamber, depth 560 μm. Excitation wavelength 780 nm.

To further improve the photon collection efficiency and also estimate the loss of scattered fluorescence photons that reached the sample surface opposite to the detector and escaped the sample, we applied a mirror on the surface to reflect the photons back into the sample and to the detector.

Figure 4a shows the experimental scheme. A tissue phantom with embedded fluorescent beads was imaged at various depths. Images of the same beads were acquired with and without the mirror placed on the top surface of the sample, using identical excitation power levels. Figure 4b shows the ratio of the fluorescence intensities for the beads imaged with and without the mirror, plotted against imaging depth. It can be seen that the mirror increases the image intensity by about 30% with a slight decrease with imaging depth. This demonstrates that the simple addition of a mirror on top of the sample surface makes it possible to improve image intensity and, as a result, also to increase the imaging depth in our detection method.

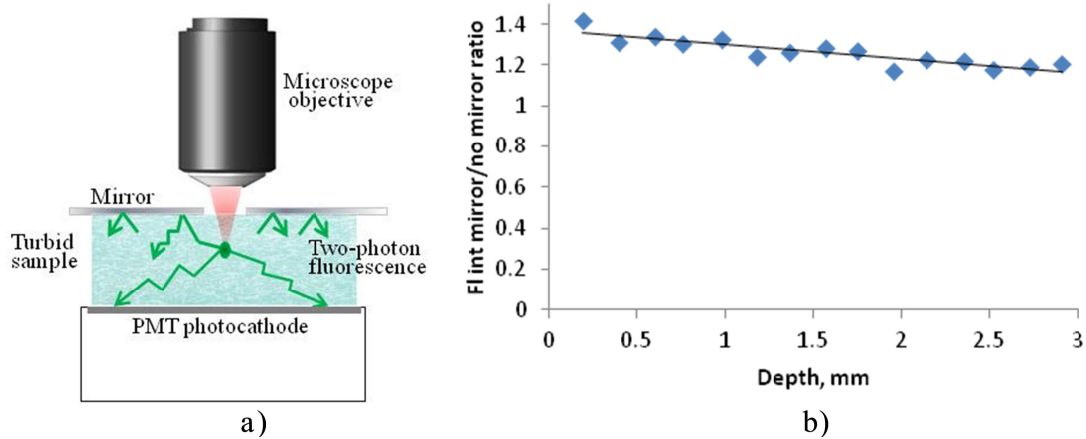


Figure 4. (a) Experimental setup. A mirror is placed on top of the sample to reflect the fluorescence photons, which would otherwise be lost, back to the detector; (b) Ratio of image fluorescence intensity of the turbid sample with and without mirror on its surface.

### 3.2 SHG imaging

SHG is a very useful imaging technique that has been successfully used in the imaging of biological tissues both *ex vivo* and *in vivo* [6]. Because SHG photons propagate mainly in the same direction as the excitation light, our detection scheme, working in transmission geometry, is naturally very suitable and more sensitive for detecting SHG signals than conventional microscopes, which have to collect back scattered SHG photons of much lower intensity and thus require higher excitation powers for imaging.

To demonstrate the performance of our detection method in acquiring of SHG images and compare it with the traditional epi-detection scheme, we have imaged several samples generating SHG signals using both detection schemes at the same time.

Urea crystals are known to give a very strong second harmonic signal [23]. We have imaged samples containing dispersed urea crystals and compared the SHG signals in the epi- and transmission geometry. Figure 5 shows the SHG images of urea crystals dispersed in a clear (non-scattering) silicone resin sample. At a given excitation power level (3 mW), the image acquired by the trans- PMT is very bright (Fig. 5a), while the epi-PMT barely senses any light (Fig. 5b). In order to see an image of the crystal acquired by the epi- PMT, the excitation power had to be increased by 10-fold

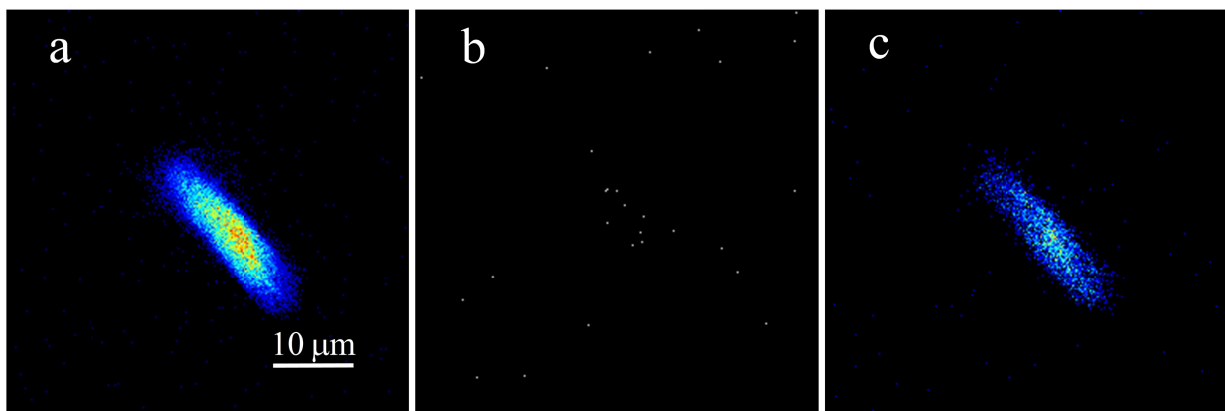


(Fig.5c).

Figure 5. SHG images of urea crystals dispersed in a clear (non-scattering) silicone matrix. Images (a-b) were acquired by the trans-PMT and epi-PMT respectively at 3 mW excitation power. Image (c) was acquired by the epi-PMT at 30 mW excitation power. Excitation wavelength 800 nm.

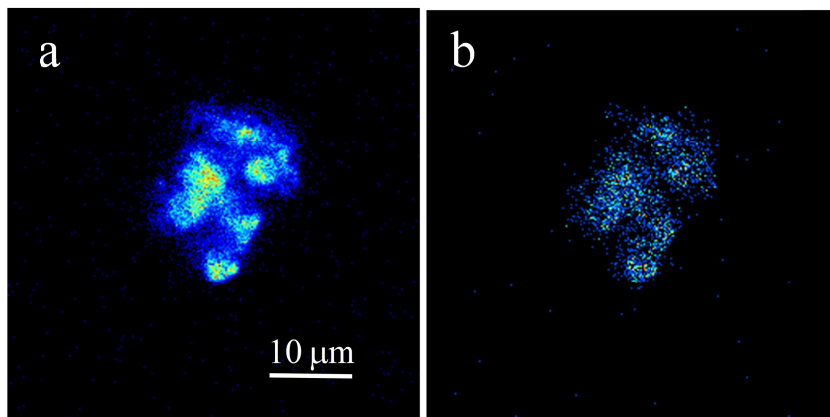


Figure 6. SHG images of urea crystals dispersed in a scattering silicone matrix acquired by trans-PMT (a) and epi-PMT (b). Excitation wavelength 800 nm.

Figure 6 shows the images of urea crystals in a scattering silicone sample at the depth of 1.2 mm. At the same power level, the intensity of the images acquired by the trans-PMT (Fig. 6a) is higher than the one acquired by the epi-PMT (Fig. 6b) and the ratio of image intensities was measured to be 50:1. The SHG signal can still be detected by the epi-

PMT because the SHG photons are redirected by multiple scattering to the epi-detector. Still, because the scattering is preferentially forward directed, the SHG detection efficiency of the trans-PMT appears to be much higher.

Collagen, which is widely present in the ECM of biological tissues, gives SHG signal due to its structure lacking a centre of symmetry. Figure 7 shows the images of collagen fibers acquired by both PMTs. The image acquired by the trans-PMT (Fig.7a) appears much more intense than the one acquired by the epi-PMT (Fig. 7b). The ratio of the intensities of these images was measured to be  $\sim 250:1$ .

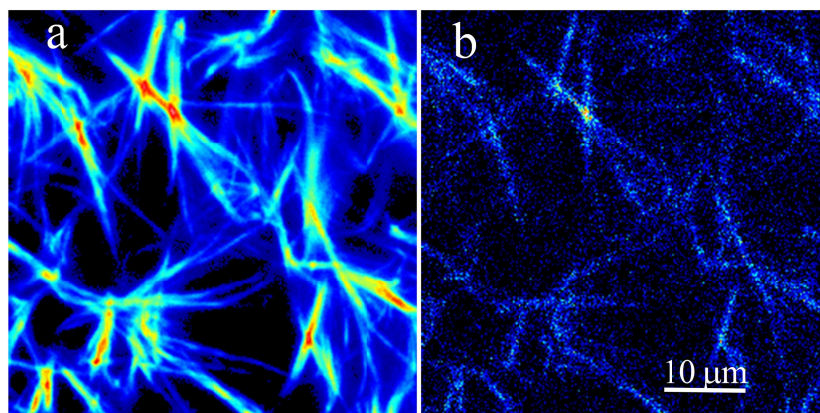


Figure 7. Collagen matrix imaged by the trans-PMT (a) and epi-PMT (b). Excitation wavelength 800 nm.

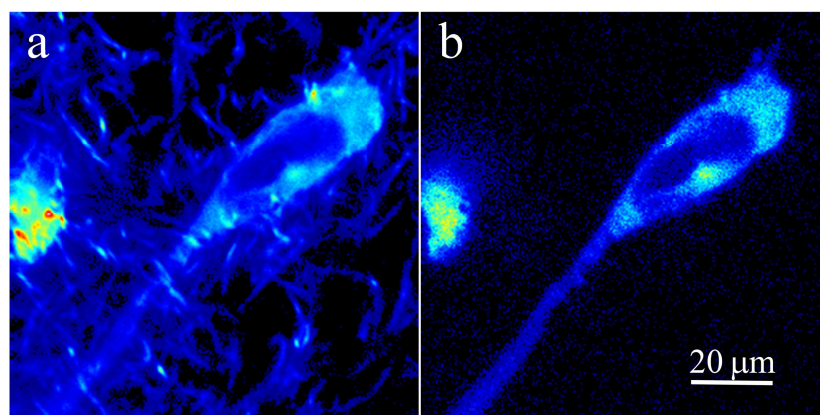


Figure 8. Fluorescence and SHG images of the collagen matrix embedded with fluorescent labeled MDA-MB-231 cells acquired by the trans-PMT (a) and by the epi-PMT (b). Excitation wavelength 860 nm.

Figure 8 shows images acquired at 1.2 mm depth of a collagen matrix embedded with fluorescently labeled paxillin MDA-MB-231 cells. While the isotropic fluorescence signal emitted by the cells is comparable on both detectors, the images of collagen fibers could only be acquired with the trans-PMT at a given excitation power level.

### 3.3 Fluorescence Lifetime Imaging Microscopy (FLIM)

We have demonstrated the capabilities of our system to acquire FLIM images in depths exceeding those achievable by conventional microscopes. To the best of our knowledge, FLIM data have not been reported at such depths. More detailed data on our system's FLIM performance will be described elsewhere. Figure 9 shows in-depth FLIM imaging of fluorescent beads of different color and size dispersed in a scattering silicone tissue phantom. Figure 9a shows a 10  $\mu\text{m}$  red bead at the depth of 1.2 mm, while figure 9b shows a 15  $\mu\text{m}$  yellow-green fluorescent bead at the depth of 3 mm. Figure 9c shows the phasor-plot of the image. It can be clearly seen how the two lifetimes are very well separated and discernible. The beads can be highlighted according to their lifetimes.

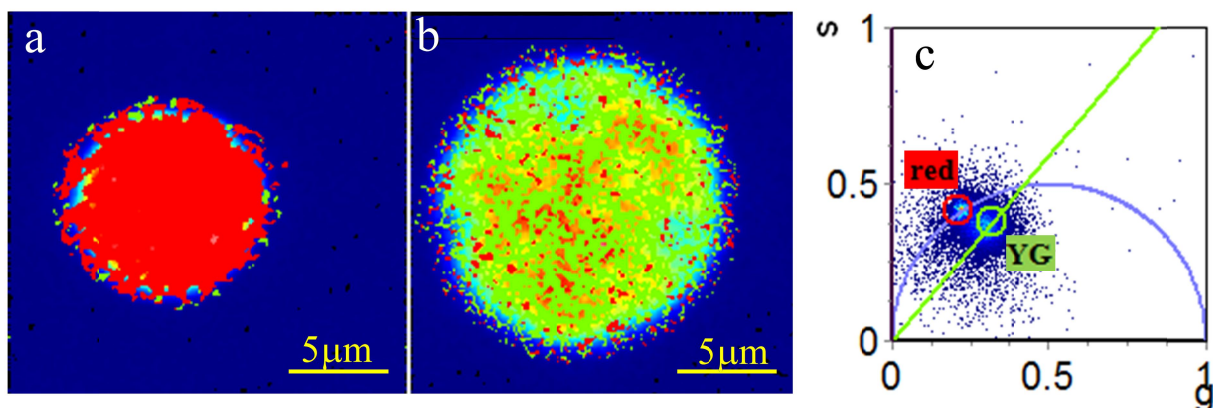


Figure 9. FLIM images of fluorescent beads dispersed in a scattering silicone sample: a) 10  $\mu\text{m}$  fluorescent red bead at 1.2 mm depth. b) 15  $\mu\text{m}$  yellow-green fluorescent bead at 3 mm depth, excitation wavelength 800nm. c) phasor-analysis of lifetimes.

#### 4. CONCLUSIONS

We presented a two-photon fluorescence scanning microscope that, due to its innovative detection system, allows fluorescence and SHG imaging in turbid biological and non-biological media, up to the depth of a few millimeters with micron resolution. The detector harvests photons from wide area of the sample with minimum photon losses. The optical path between the sample and the detector is completely refractive-index matched, curtailing losses due to reflections at the boundaries. This system is very sensitive to low-level signals and allows imaging at extended depths.

The system transmission geometry has an advantage in the detection of SHG signals that intrinsically tend to propagate in the direction of the excitation light. The system also has in-depth FLIM capabilities, and efficiently separates images based on different lifetimes up to the depth of 3mm. The optical sectioning and SHG detection capabilities of the system make it very suitable for biological imaging and medical diagnostics.

#### ACKNOWLEDGEMENTS

This work was supported by National Institutes of Health grant: 8P41GM103540. The authors would like to thank Dr. C Stringari, Dr. W.W. Mantulin, Chi-Li Chiu, Dr. R. Saager, Dr. B. Choi, S. White, Dr. R. Edwards, Dr. M. Waterman for providing us with the samples.

#### REFERENCES

- [1] O'Malley, D., "Imaging in Depth: Controversies and Opportunities," *Methods in Cell Biology*, Vol. 89, Ch. 5, 95-128 (2008).
- [2] Theer, P., Hasan, M. T., and Denk, W., "Two-photon imaging to a depth of 1000 micron in living brains by use of a Ti:Al<sub>2</sub>O<sub>3</sub> regenerative amplifier," *Opt. Lett.* 28(12), 1022-1024 (2003).
- [3] Kobat, D., Durst, M. E., Nishimura, N., Wong, A. W., Schaffer, C. B., and Xu, C., "Deep tissue multiphoton microscopy using longer wavelength excitation," *Opt. Express* 17, 13354– 13364 (2009).

- [4] Cicchi, R., Sampson, D.D., Massi, D., and Pavone, F. S., "Contrast and depth enhancement in two-photon microscopy of human skin *ex vivo* by use of optical clearing agents," *Opt. Express* 13, 2337-2344 (2005).
- [5] Combs, C. A., Smirnov, A. V., Riley, J. D., Gandjbakhche, A. H., Knutson, J. R., and Balaban, R. S., "Optimization of multiphoton excitation microscopy by total emission detection using a parabolic light reflector," *J. Microsc.* 228, 330-337 (2007).
- [6] Campagnola, P. J., Dong, C. "Second harmonic generation microscopy: principles and applications to disease diagnosis", *Laser Photonics Rev.* 5, No. 1, 13–26 (2011).
- [7] Zipfel, W. R., Williams, R. M., Watt, W. W., "Non-linear magic: multiphoton microscopy in the biosciences" *Nature Biotechnology*, 21(11), 1369-1377 (2003).
- [8] Chen, X., Raggio, C., and Campagnola, P. J., "Second-harmonic generation circular dichroism studies of osteogenesis imperfecta," *Opt Lett.*, 37(18) (2012).
- [9] Nadiarnykh, O., LaComb, R. B., Brewer, M. A., Campagnola, P. J., "Alterations of the extracellular matrix in ovarian cancer studied by Second Harmonic Generation imaging microscopy" *BMC Cancer*, 10:94 (2010).
- [10] Ajeti, V., Nadiarnykh, O., Ponik, S. M., Keely, P. J., Eliceiri, K. W., Campagnola, P. J., "Structural changes in mixed Col I/Col V collagen gels probed by SHG microscopy: implications for probing stromal alterations in human breast cancer," *Biomedical Optics Express*, Vol. 2, No. 8. (2011).
- [11] Plotnikov, S. V., Kenny, A. M., Walsh, S. J., Zubrowski, B., Joseph, C., Scranton, V. L., Kuchel, G. A., Dauser, D., Xu, M., Pilbeam, C. C., Adams, D. J., Dougherty, R. P., Campagnola, P. J., Mohler, W. A. "Measurement of muscle disease by quantitative second-harmonic generation imaging" *Journal of Biomedical Optics* 13(4) (2008).
- [12] Ishikawa-Ankerhold, H. C., Ankerhold, R., and G. P. C. Drummen, G. P. C., "Advanced Fluorescence Microscopy Techniques—FRAP, FLIP, FLAP, FRET and FLIM," *Molecules*, 17, 4047-4132 (2012).
- [13] Bastiaens, P. I., Squire, A., "Fluorescence lifetime imaging microscopy: spatial resolution of biochemical processes in the cell," *Trends Cell Biol.*, 9, 48–52 (1999).
- [14] van Munster, E. B., Gadella, T. W., Jr., "Suppression of photobleaching-induced artifacts infrequency-domain FLIM by permutation of the recording order," *Cytometry A*, 58, 185–194 (2004).
- [15] Digman, M. A., Caiolfa, V. R., Zamai, M., and Gratton, E., "The Phasor approach to fluorescence lifetime imaging analysis". *Biophys J.*, 94(2) (2008).
- [16] Crosignani, V., Dvornikov, A. S., and Gratton, E., "Enhancement of imaging depth in turbid media using a wide area detector," *J. Biophotonics* 4(9), 592–599 (2011).
- [17] Crosignani, V., Dvornikov, A. S., Aguilar, J. S., Stringari, C., Edwards, R., Mantulin, W. W., and Gratton, E., "Deep tissue fluorescence imaging and *in vivo* biological applications," *Journal of Biomedical Optics*, 17(11) (2012).
- [18] Ayers, F., Grant, A., Kuo, D., Cuccia, D. J., and Durkin, A. J., "Fabrication and characterization of silicone-based tissue phantoms with tunable optical properties in the visible and near infrared domain," *Proc. SPIE* 6870, 687007-1-9 (2008)
- [19] Stringari, C., Edwards, R. A., Pate, K. T., Donovan, P. J., Waterman, M. L., and Gratton, E., "Metabolic trajectory of cellular differentiation in small intestine by phasor fluorescence lifetime microscopy of NADH," *Sci Rep*, 2: 568 (2012).
- [20] Moy, A. J., White, S. M., Indrawan, E. S., Lotfi, J., Nudelman, M. J., Costantini, S. J., Agarwal, N., Jia, W., Kelly, K. M., Sorg, B. S., and Choi, B., "Wide-field functional imaging of blood flow and hemoglobin oxygen saturation in the rodent dorsal window chamber," *Microvascular Research* 82, 199–209 (2011).
- [21] Yaroslavsky, A. N., Schulze, P. C., Yaroslavsky, I. V., Schober, R., Ulrich, F., and Schwarzmaier, H. J., "Optical properties of selected native and coagulated human brain tissues *in vitro* in the visible and near infrared spectral range," *Phys. Med. Biol.*, 47, 2059–2073(2002).
- [22] He, G., Shankar, R. A., Chczhan, M., Samouilov, A., Kappusamy, P., and Zweier, J. L., "Noninvasive measurement of anatomic structure and intraluminal oxygenation in the gastrointestinal tract of living mice with spatial and spectral EPR imaging," *Proc. Natl. Acad. Sci.*, 96, 4586–4591, (1999).
- [23] Romani, S., Razzetti, C., Zha, M., Paorici, C., "Evaluation of the Effective Second Harmonic Generation Coefficient of Monomethyl Urea Single Crystals" *phys. stat. sol. (b)* 197, 271 (1996).